Journal of the Serbian Chemical Society
JSCS-info@shd.org.rs • www.shd.org.rs/JSCS

# ACCEPTED MANUSCRIPT

Journal of the Serbian Chemical Society
JSCS-info@shd.org.rs • www.shd.org.rs/JSCS
*J. Serb. Chem. Soc.* **00(0)**1-14 (2023)
*JSCS–12534*
*Original scientific paper*
Published DD MM, 2023



# Chemical reactivity of alliin and its molecular interactions with the M protease$^{pro}$ of SARS-CoV-2

WENDOLYNE LÓPEZ-OROZCO, LUIS HUMBERTO MENDOZA-HUIZAR*, GIAAN ARTURO ÁLVAREZ-ROMERO, JESÚS MARTÍN TORRES-VALENCIA, AND MARICRUZ SANCHEZ-ZAVALA

*Academic Area of Chemistry, Universidad Autónoma del Estado de Hidalgo, Carretera Pachuca-Tulancingo, 42184, Mineral de la Reforma, Hidalgo, Mexico*

(Received 17 August; Revised 9 September; Accepted 11 October 2023)

*Abstract:* In the present work a computational study of the chemical reactivity of alliin at the X/DGDZVP level of theory (where X=B3LYP, M06, M06L and wB97XD) was performed. The distribution of active sites on alliin was determined by evaluating the Fukui function. For electrophilic attacks, the more reactive sites are on the carbon atoms of the prop-2-ene moiety. The more active sites for nucleophilic attacks are located on the thioether group. In the case of free radical attacks, the more reactive sites are on the carbonyl, thioether and prop-2-ene moieties. Additionally, the molecular docking study revealed that, alliin is able to dock to the Mprotease$^{pro}$ of SARS-CoV-2 through interactions with the catalytic CYS145-HSD164 dyad via Van der Waals interactions, with MET49 with interactions alkyl-type ions and with PHE140 by hydrogen bonds. Also, the molecular dynamic study indicates that alliin remains in the pocket site. Last result suggests that this molecule is a potential candidate for further in vitro evaluation as a drug for the treatment of the major protease-based SARS-CoV-2 virus.

*Keywords:* Fukui function; molecular docking, non-covalent.

## INTRODUCTION

Alliin (2-amino-3-prop-2-enylsulfanylpropanoic acid), is the most important sulfur compound present in garlic *allium sativum.*[1] It is well known that alliin is a bioactive compound with medicinal activity, and its organosulfur compounds serve as important storage peptides and synthetic intermediates.[2] Alliin has shown anticarcinogenic[3] and antibiotic activity.[4] In addition, alliin exhibit cardio and neuroprotective actions and is able to suppress inflammatory responses.[2] Also, its antiviral activity has been studied for herpes simplex type 1 and 2, influenza type

* Corresponding author E-mail: hhuizar@uaeh.edu.mx
https://doi.org/10.2298/JSC230817078L

3, vaccinia virus, stomatitis, vesicular and human rhinovirus, however, at working concentrations, it has presented cytotoxicity by which is necessary to extend the study.[5] Additionally, alliin and its derived sulfoxides have shown a mechanism of action that prevents the formation of free radicals by electron capture, which gives rise to its antioxidant activity.[6] Also, it has been evaluated as an inhibitor of SARS-CoV-2 $M^{pro}$ through molecular docking analysis,[7] and molecular dynamics.[7] It was found that the formation of hydrogen bonds between this serine- type protease and alliin in the active site regions inhibits the COVID-19 outbreak.[7] Here, it is important to mention that the ΔG energy of antigen-receptor binding represents the basis of the virus-host interaction at the cell surface, which allows the virus to enter its host cell. Thus, in order to infect a host cell, a virus must have an antigen (for example, the spike glycoprotein of SARS-CoV-2) that has a negative ΔG energy of binding to the host cell receptor (e.g., the ACE2 receptor for SARS-CoV-2). Thus, thermodynamic and kinetic studies play an important role in the evaluation of antiviral agents because of the complexes formed by virus receptors with the study agent.[8,9] In this sense, these kinds of studies related to the formation of the aliin-$M^{pro}$ complex have allowed to evaluate the binding of the complex for different Omicron variants of SARS-CoV-2.[10] Since the binding ΔG plays an important role in determining the stability of the complex with which viral infectivity and mutability may be evaluated. Thus, the bioinformatics studies reported in the literature suggest that alliin may be used alone or in combination with the main therapeutic drug, which would be an efficient therapy to eradicate SARS-CoV-2 with the lowest side effects and toxicity.[7,11] Nevertheless, no drugs have been developed based on the potential of this bioactive molecule because it is necessary more information related to the alliin-receptor binding. Additionally, we consider that the determination of alliin electronic properties would allow understanding the therapeutic effect towards different diseases. In this sense, to the best of our knowledge, only different sulfur derivatives of alliin have been studied from theoretical point of view employing semiempirical methods[12] and ab initio methods in order to investigate their structural properties, vibrational modes and electronic structure.[13] Thus, in the present work, we evaluate the global and local reactivity parameters of alliin, the binding energy of the complex alliin-$M^{pro}$, and validate the docking analysis with a molecular dynamic study. We believe that this type of study contributes to a better understanding of the chemical behavior of this important bioactive compound.

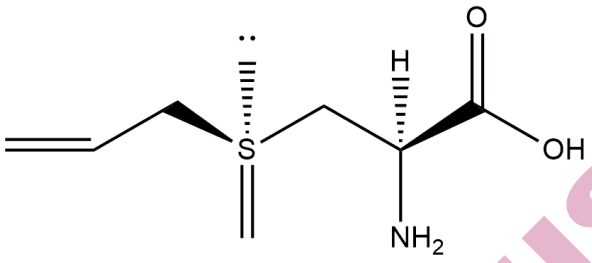


Figure 1. Structure of alliin (2-amino-3-prop-2-enylsulfanylpropanoic acid).

## THEORY

Within the framework of density functional theory, it is possible to derive parameters that can be used to analyze the reactivity of a molecular system, such as: the electronic chemical potential (μ), electronegativity (χ), hardness (η), and the electrophilicity index (ω).[14]

$$\mu = \left(\frac{\partial E}{\partial N}\right)_{v(r)} = -\frac{1}{2}(I + A) = \frac{1}{2}(\varepsilon_L + \varepsilon_H) = (\varepsilon_L - \varepsilon_H) \quad (1)$$

$$\chi = -\mu \quad (2)$$

$$\eta = \left(\frac{\partial \mu}{\partial N}\right)_{v(r)} = \left(\frac{\partial^2 E}{\partial N^2}\right)_{v(r)} = (I - A) = (\varepsilon_L - \varepsilon_H) \quad (3)$$

$$\omega = \frac{\mu^2}{2\eta} \quad (4)$$

In these equations, $E$, $N$ and $v(r)$are the energy, the number of electrons and the external potential exerted by the nuclei, respectively. $I$ is the ionization potential and A corresponds to the electronic affinity. $\varepsilon_L$ is the energy of the lowest unoccupied molecular orbital (LUMO), while $\varepsilon_H$ is the energy of the highest occupied molecular orbital (HOMO).[15] The electronic chemical potential is related with the electronic escape tendency[16]. The hardness is related to the stability of molecular systems[17] because it allows measuring the chemical susceptibility of the species to accept electrons.[13] The electrophilicity index suggests a good nucleophile for higher values, while it indicates the presence of a good electrophile at higher values. In addition, it is possible to define the powers of electroacceptance ($\omega^-$) and eletrodonation ($\omega^+$).[13]

$$\omega^- = \frac{(\mu^-)^2}{2\eta} = \frac{\left(-\frac{1}{4}(3I+A)\right)^2}{2(I-A)} = \frac{\left(-\frac{1}{4}(3\varepsilon_L+\varepsilon_H)\right)^2}{2(\varepsilon_L-\varepsilon_H)} \quad (5)$$

$$\omega^+ = \frac{(\mu^+)^2}{2\eta} = \frac{\left(-\frac{1}{4}(I+3A)\right)^2}{2(I-A)} = \frac{\left(-\frac{1}{4}(\varepsilon_L+3\varepsilon_H)\right)^2}{2(\varepsilon_L-\varepsilon_H)} \quad (6)$$

Also, the Fukui function, $f(\mathrm{r})$, is a local parameter commonly used to identify regions of increased activity on a molecular system,[18] and is defined as follows:[18]

$$f(r) = \left(\frac{\partial \rho(r)}{\partial N}\right)_{v(r)} = \left(\frac{\partial \mu(r)}{\partial v(r)}\right) \quad (7)$$

where, $\rho$(r) is the electron density. Note that equation (7) allows us to identify the regions in which the electron density is modified by varying the number of electrons, which is useful for identifying the molecular regions most susceptible to nucleophilic and electrophilic attacks.[19] Also, it is possible to evaluate FF by using different approaches which are: a) frozen core approximation (FC)[18], b) finite differences (FD)[18], and c) finite differences employing atomic charges (FDAC).[20] Under the FC approximation, FF is evaluated as:

$$f^{-}(r) = \varphi_H^*(r)\varphi_H(r) = \rho_H(r) \quad (8)$$

$$f^{+}(r) = \varphi_L^*(r)\varphi_L(r) = \rho_L(r) \quad (9)$$

where $f^{-}$( r ) and $f^{+}$( r ) correspond to electrophilic and nucleophilic attacks, respectively, $\rho_H$(r) is the electron density of the HOMO orbital, and $\rho_L$(r) is the electron density of the LUMO orbital. In the case of FD and FDAC approximations, it is possible to define the FF for electrophilic, nucleophilic and free radical attacks $f^0$( r ). Thus, in the FD approximation, FF is determined as

$$f^{-}(r) = \rho_N(r) - \rho_{N-1}(r) \quad (10)$$

$$f^{+}(r) = \rho_{(N+1)}(r) - \rho_N(r) \quad (11)$$

$$f^{0}(r) = \frac{1}{2}[\rho_{N+1}(r) - \rho_{N-1}(r)] \quad (12)$$

where $\rho_{N+1}$(r), $\rho_N$(r), and $\rho_{N-1}$(r) correspond to the electron density of the anionic, neutral and cationic species, respectively. In the third approximation (FDAC), $q_j$ is the atomic charge at the $j_{ésimo}$ site for neutral (N), anionic (N+1), or cationic (N-1) of the chemical species.

$$f_j^{-}(r) = q_{j(N-1)} - q_{j(N)} \quad (13)$$

$$f_j^{+}(r) = q_{j(N)} - q_{j(N+1)} \quad (14)$$

$$f_j^{0}(r) = \frac{1}{2}\left[q_{j(N-1)} - q_{j(N+1)}\right] \quad (15)$$

## EXPERIMENTAL

The alliin structure was subjected to full geometric optimization in the aqueous phase employing the X / DGDZVP level of theory.[21] (where X = B3LYP,[22] M06,[23] M06L,[24] and ωB97XD[25]). Solvent phase optimization was carried out using the continuous polarizable model (PCM) developed by Tomasi et al.[26] In all cases, vibrational frequencies were calculated to ensure that the stationary points were minimal on the potential energy surface. All quantum calculations reported here were performed with the Gaussian program 09[27] program, and visualized with the packages GaussView,[28] Gabedit[29] and Multwfn [30]. The docking study was performed through the Swiss Bioinformatics Institute website with the free software SwissDock[31]. Visualizations of the ligand/receptor complex were performed in the programs Chimera[32] and Discovery Studio Visualizer 2019.[33]

## RESULTS AND DISCUSSION

The alliin structure was optimized without restrictions at the X/DGDZVP level of theory at gas and aqueous phase.[3] (where X = B3LYP,[22] M06,[23] M06L,[24] and ωB97XD[25]), see Figure 2. Here, it is important to mention that no significant differences were obtained, neither in distances nor in angles, when the solvent effect was considered at the different levels of theory employed in this work. All the frequency values calculated at the theoretical level X / DGDZVP[21] in both phases were positive and are in good agreement with the values reported in the literature, suggesting that the level of theory employed is able to predict the electronic properties of alliin. A summary of the main bands for the aqueous phase present in the alliin spectrum is shown in Figure S-1 of the supplementary material which are at 270 $cm^{-1}$ for the N-H bending out of plane, 580 $cm^{-1}$ O-H bending out of plane, 970 $cm^{-1}$ S=O stretching, 1160 $cm^{-1}$ N-C stretching, 3060 $cm^{-1}$ C-H stretching, 3500 $cm^{-1}$ N-H stretching and 3690 $cm^{-1}$ O-H stretching.

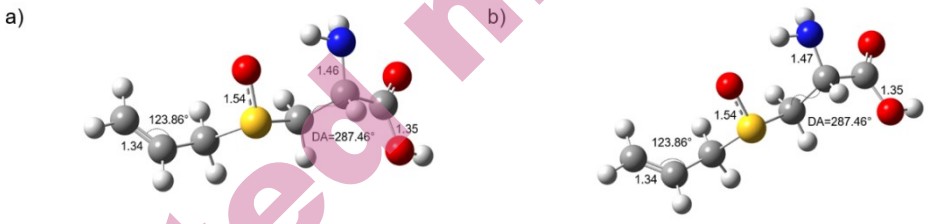


Figure 2. Structure of alliin (a) gas phase and (b) aqueous phase, optimized at the B3LYP/DGDZVP level of theory in the aqueous phase using the PCM solution model. Bond distances are given in Angstroms, DA=DihedralAngle.

*Global reactivity descriptors*

The global reactivity descriptors for alliin were evaluated using equations (1)-(6) and are reported in Table 1. The electronic chemical potential values indicate that alliin is a good nucleophile. It is also a stable molecule according to the hardness values obtained at all levels of theory. Note that the presence of solvent has no effect on the global chemical reactivity of alliin.

Table 1. Global reactivity parameters calculated for alliin, evaluated at the X/DGDZVP level of theory (where X=B3LYP, M06, M06L, and ωB97XD) in aqueous and gas phases, using equations (1)-(6). Values in parentheses correspond to the values calculated using Koopmans theorem.

| **Aqueous** | **I / eV** | **A / eV** | **μ / eV** | **μ / eV** | **$\mu^-$** | **$\mu^+$** | **χ / eV** | **ω / eV** | **$\omega^+$ / eV** | **$\omega^-$ / eV** |
|---|---|---|---|---|---|---|---|---|---|---|
| **B3LYP** | 6.76 | 0.94 | -3.85 | 5.81 | -6.76 | -0.94 | 3.85 | 1.27 | 0.08 | 3.93 |
| | (-0.83) | (-6.76) | (3.80) | (5.92) | (0.83) | (6.76) | (-3.80) | (1.22) | (3.85) | (0.06) |
| **M06** | 6.89 | 0.82 | -3.86 | 6.07 | -6.89 | -0.82 | 3.86 | 1.22 | 0.06 | 3.91 |
| | (-0.51) | (-7.07) | (3.79) | (6.56) | (0.51 | (7.07) | (-3.79) | (1.09) | (3.81) | (0.02) |
| **M06L** | 8.64 | 0.96 | -4.80 | 7.68 | -8.64 | -0.96 | 4.80 | 1.50 | 0.06 | 4.86 |
| | (0.96) | (-5.89) | (2.46) | (6.85) | (-0.96) | (5.89) | (-2.46) | (0.44) | (2.53) | (0.07) |
| **WB97XD** | 6.92 | 0.33 | -3.63 | 6.59 | -6.92 | -0.33 | 3.63 | 1.00 | 0.01 | 3.63 |
| | (1.28) | (-8.90) | (3.81) | (10.18) | (-1.28) | (8.90) | (-3.81) | (0.71) | (3.89) | (0.08) |
| **Gas** | | | | | | | | | | |
| **B3LYP** | 6.75 | 0.96 | -3.86 | 5.79 | -6.75 | -0.96 | 3.86 | 1.28 | 0.08 | 3.93 |
| | (-0.86) | (-6.76) | (3.81) | (5.90) | (0.86) | (6.76) | (-3.81) | (1.23) | (3.87) | (0.06) |
| **M06** | 6.90 | 0.83 | -3.86 | 6.07 | -6.90 | -0.83 | 3.86 | 1.23 | 0.06 | 3.92 |
| | (-0.51) | (-7.07) | (3.79) | (6.56) | (0.51) | (7.07) | (-3.79) | (1.09) | (3.81) | (0.02) |
| **M06L** | 9.05 | 0.96 | -5.01 | 8.09 | -9.05 | -0.96 | 5.01 | 1.55 | 0.06 | 5.06 |
| | (-1.26) | (-5.89) | (3.58) | (4.62) | (1.26) | (5.89) | (-3.58) | (1.38) | (3.75) | (0.17) |
| **WB97XD** | 6.92 | 0.33 | -3.62 | 6.59 | -6.92 | -0.33 | 3.62 | 1.00 | 0.01 | 3.63 |
| | (1.28) | (-0.89) | (-0.20) | (2.17) | (-1.28) | (0.89) | (0.20) | (0.01) | (0.18) | (0.38) |

*Local reactivity parameters*

The local reactivity of a molecular system can be evaluated through the Fukui Function, using the FC and FD approximations. Figure 3 shows the distribution of the electrophilic sites in alliin, using the FC approximation in the aqueous phase, it is worth mentioning that a similar behavior was observed in the gas phase (See Figure S-2). Note that for alliin the HOMO distribution is localized over the sulfoxide and the alkene, while the LUMO distribution is localized over the whole molecule except for the nitrogen bonded hydrogens.

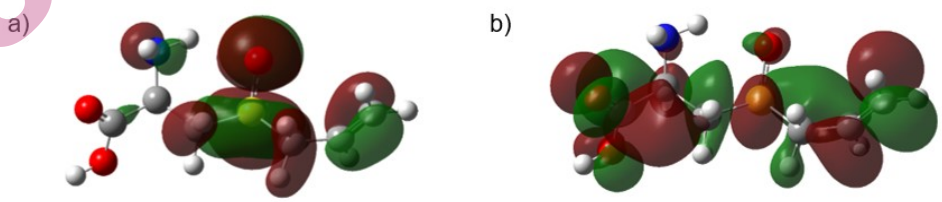


Figure 3. HOMO and LUMO distributions on alliin obtained at the B3LYP/DGDZVP level of theory in the aqueous phase using the PCM solution model. In all cases the isosurfaces were obtained at 0.08 e/u.a.$^3$.

The evaluation of the Fukui Function using the FD approximation (equations (10)-(12)) in the aqueous phase is reported in Figure 4 for alliin. The most active

sites towards nucleophilic attacks are found at 1C, 2C and 9C (Figure 4a), on the alkene carbons. For electrophilic attacks, the most reactive sites are found at positions 3C, 4S and 5O (Figure 4b), in the thioether region, while for free radical attacks the most reactive sites are the same sites as the total for nucleophilic and electrophilic attacks (Figure 4c). It is clear from the FD approach that the most reactive sites are located in the same positions for the gas and aqueous phase, which is indicative that they are showing the same reactivity to the different types of attacks (See Figure S-3).

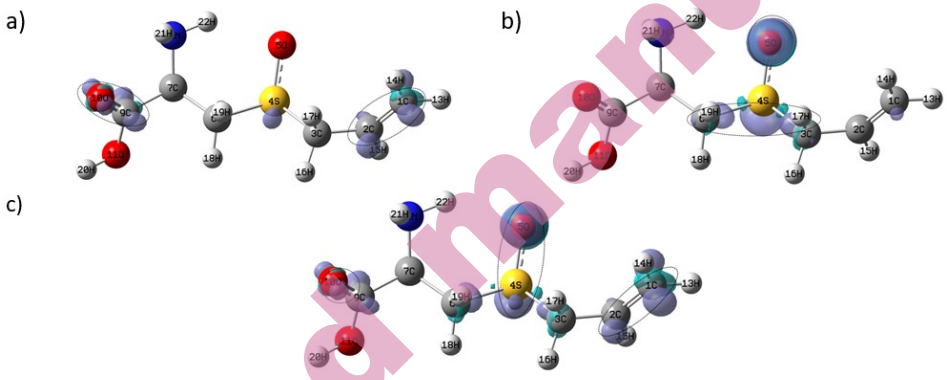


Figure 4. Isosurfaces of Fukui Functions for alliin according to equations (10), (11) and (12) at the B3LYP/DGDZVP level of theory using the PCM solution model. In the case of (a) nucleophilic, (b) electrophilic and (c) free radical attacks. In all cases the isosurfaces were obtained at 0.008 e/a.u. [3]The dotted circles show the most reactive zones in each molecule.

Furthermore, it is possible to condense the Fukui function through equations (13)-(15) to identify the point distribution of the active sites because the highest values of CFF correspond to the most reactive atoms in the reference molecule.[4] In the case of equations (13)-(15), we used the Hirshfeld population to evaluate the CFF values because the values obtained are non-negative.[35,36] The CFF values for nucleophilic attacks at the different levels of theory, for alliin calculated in aqueous phase, are shown in Figure 5. Note that alliin exhibits the most susceptible sites towards nucleophilic attacks at 1C, 2C and 9C. In the case of electrophilic attack, the most reactive sites are 3C, 4S and 5O (Figure S-4). Whereas, the most reactive sites towards a free radical attack are 1C, 9C, 4S and 5O (Figure S-5). It was also observed that the molecule has the same behavior in the gas phase (Figures (S-6)-(S-8)).

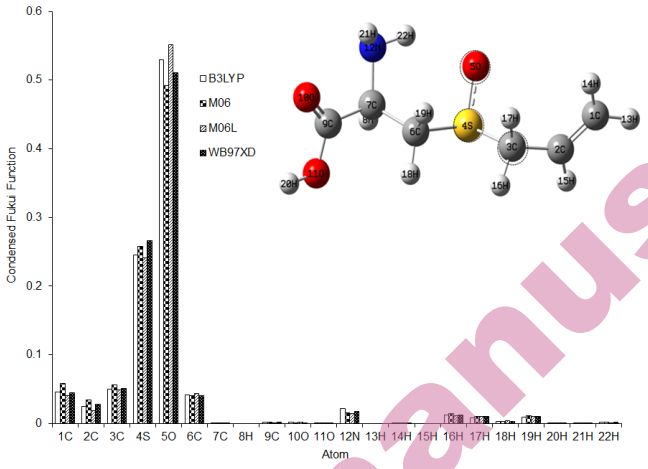


Figure 5. Condensed Fukui function values for nucleophilic attacks on alliin at the X/ DGDZVP level of theory (where X=B3LYP, M06, M06L and ωB97XD), in the aqueous phase using the Hirshfeld population and equations (12)-(14), the dotted circles show the most reactive zones in each molecule.

In addition to global and local reactivity descriptors, it is possible to analyze chemical reactivity through molecular electrostatic potential (MEP) maps.[31] Figure 6 shows the MEPs of the alliin molecule. In this image, the negative potential areas (red color) are characterized by an abundance of electrons while the positive potential areas (blue color) are characterized by a relative lack of electrons. Alliin exhibits the highest potential values on hydrogen and nitrogen atoms compared to the other atoms; therefore they have a lower electron density around them, and show that oxygen atoms are the sites with the lowest potential and therefore are the most electrophilic active sites. The same occurred when performing the PEM for almotriptan in the gas phase, as shown in Figure S-9.

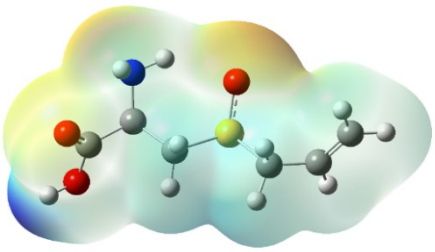

Figure 6. Mapping of the electrostatic potentials evaluated at the B3LYP/DGDZVP level of theory using the PCM solvation model, on a density isosurface (value =0.002 e/a.u.$^3$) for alliin.

*Non covalent interactions*

As expressed by the NCI index, in regions far from the molecule, the density decreases to zero exponentially and, consequently, the reduced gradient will have large positive values, while in regions of covalent bonding and non-covalent interactions, the reduced gradient will have values close to zero.[37]

$$s(r) = \frac{1}{2(3\pi^2)^{1/3}} \frac{|\nabla\rho(r)|}{\rho(r)^{4/3}} \quad (16)$$

Figure 7 shows this plot for alliin, note that, in the low reduced gradient region, several interactions are observed, caused by the interactions in the amide. To verify this result, the isosurface s(r) of the alliin structure was plotted, see Figure S-10.

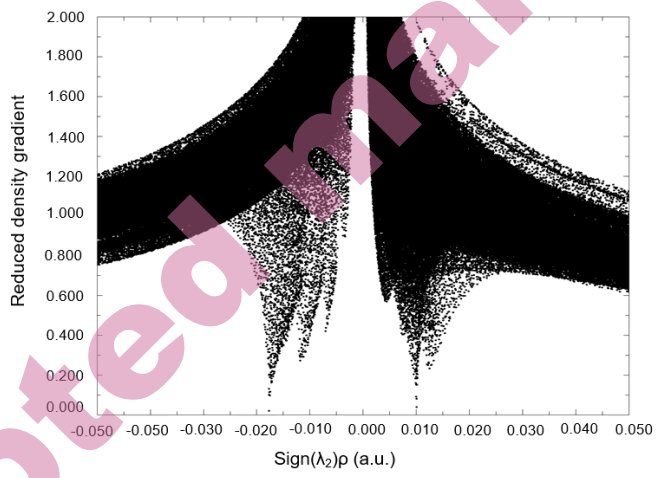


Figure 7. Plot of the reduced density gradient vs sign($\lambda_2$ )ρ for alliin in the aqueous phase.

*Molecular docking*

In order to analyze the influence of alliin structure on its role as an inhibitor of SARS-CoV-2 virus replication for the treatment of COVID-19 disease, the optimal ligand/protein configuration and binding affinity of aliin to $M^{pro}$ were analyzed. Figure 8 shows the alliin/$M^{pro}$ configuration, where the binding energy is -29.79 kJ $mol^{-1}$. This ΔG binding energy value is more negative that the previously reported in the literature (-17.99 kJ $mol^{-1}$ ),[38] suggesting a higher affinity to the alliin to the active site of $M^{pro}$. Although, previously it was reported a molecular docking of alliin with the M $protease^{pro}$ with a ΔG binding energy equal -40.57 kJ $mol^{-1}$, it is important to mention that it was done in the presence of the inhibitor N3, and this fact may decreases the number of interactions with the active site residues.[7] To identify the interactions around 3 Å, the interactions were plotted on a 2D map as shown in Figure S-11 of the supplemental material, thus it is observed that alliin has van der Waals interactions at the catalytic site of the $M^{pro}$

reported.[39] The interaction of alliin with the catalytic site of M$^{pro}$, at residues CYS145 and HSD164, considered the catalytic dyad, in addition to ASN142, MET165, HSD163, GLU166, HSD41, alkyl-type interaction with MET49 and by hydrogen bridging with PHE140.

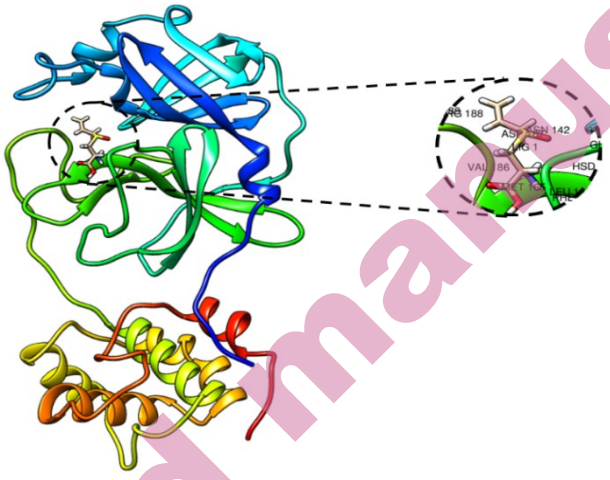

Figure 8. Alliin binding site in the M protease$^{pro}$ of SARS-CoV-2.

*Molecular dynamics simulation study*

The molecular dynamics simulation allows us to validate the docking study by evaluating the stability of the compounds docked to a protein, based on the description of the forces. Here it is important to mention that recently was reported in the literature a molecular dynamic study of 6lu7-alliin but with a RMSD larger than 2 Å, (see figure 2 in reference 12),[7] which is bigger than the average values of RMSD reported as reliable. In this work, the molecular dynamics simulation was performed for 20 ns for the M$^{pro}$ alliin complex as shown in Figure 9. The system reached equilibrium after 10 ns and fluctuated around the mean value of 0.8 Å until the end of the simulation which suggest that the formation of complex protein-ligand is stable and may inactive to the M receptor$^{pro}$.[7,40]

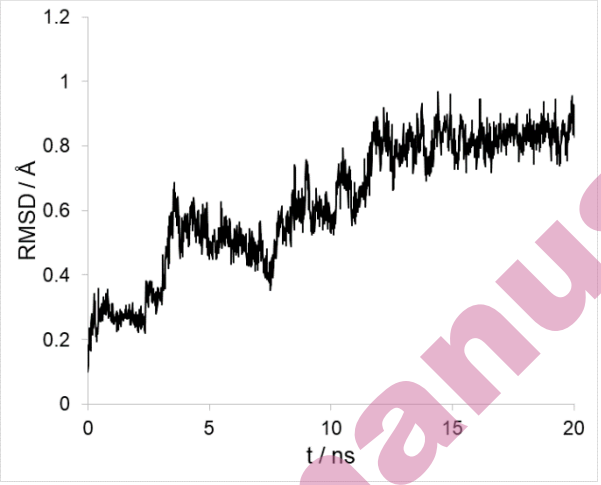


Figure 9. RMSD diagram of the SARS-CoV-2 Mpro-alliin protease complex.

## CONCLUSIONS

In the present work, the molecular chemical reactivity of the alliin structure was studied in aqueous and gas phase. Through the Fukui function it was identified that the most active sites towards nucleophiles are located at 1C, 2C and 9C for electrophilic attacks 3C, 4S and 5O and for free radical attacks the most reactive sites are the same sites as for nucleophilic and electrophilic attacks and there was no significant change in the two phases. The ΔG binding energy for the alliin/M configuration$^{pro}$ was also calculated to be equal to -29.79 kJ mol$^{-1}$. Alliin showed interactions with important residues of the active site of the M receptor$^{pro}$.

## SUPPLEMENTARY MATERIAL

Supplementary Materials are available electronically from https://www.shd-pub.org.rs/index.php/JSCS/article/view/12534, or from the corresponding authors on request.

*Acknowledgements:* WLO acknowledges CONACYT for the scholarship granted for Doctoral studies. Authors gratefully acknowledge financial support from CONACYT (project CB2015-257823) and to the Universidad Autónoma del Estado de Hidalgo. Guanajuato National Laboratory (CONACyT 123732) is acknowledged for supercomputing resources. LHMH acknowledges to the SNI for the distinction of his membership and the stipend received.

## ИЗВОД

### ХЕМИЈСКА РЕАКТИЦНОСТ АЛИИНА И ЊЕГОВА МОЛЕКУЛСКА ИНТЕРАКЦИЈА СА SARS-COV-2 M PROTEASE$^{PRO}$ -ОМ

WENDOLYNE LÓPEZ-OROZCO, LUIS HUMBERTO MENDOZA-HUIZAR, GIAAN ARTURO ÁLVAREZ-ROMERO, JESÚS MARTÍN TORRES-VALENCIA, AND MARICRUZ SANCHEZ-ZAVALA

*Academic Area of Chemistry, Universidad Autónoma del Estado de Hidalgo, Carretera Pachuca-Tulancingo, 42184, Mineral de la Reforma, Hidalgo, Mexico*

У овом раду је дата рачунарска студија хемијске реактивноисти алиина на X/DGнDZVP нивоу теорије (где је X=B3LYP, M06, M06L и wB97XD). Расподела активних места на алиину одређена је на основу Fukui-еве функције. За електрофилне нападе, најреактивнија места су на угљениковим атомима проп-2-енског дела. Реактивнија места за нуклеофилне нападе су лоцирана на тиоетарској групи. У случају слободнорадикалских напада, реактивнија места су на кабонилним, тиоетарским и проп-2-енским деловима. Додатно је студија молекулског докинга показала да је алиин у стању да пристане на Mprotease$^{pro}$ у SARS-CoV-2 кроз интеракцију са каталитичком CYS145-HSD164 дијадом преко Van der Waals-овских интеракција, са MET49 преко интеракција са јоновима алкил типа, и са PHE140 преко водоничних веза. Такође, студије молекулске динамике указују да се алиин задржава на месту цепа. Последњи резултат сугерише да је овај молекул потенцијални кандидат за даљу in vitro евалуацију као лек за третирање главног, на протеази заснованог, SARS-CoV-2 вируса.

(Примљено 17. августа 2022, ревидирано 9. септембра, прихваћено 11. октобра 2023.)

## REFERENCES

1. B. Hughes, B. Murray, J. North, L. Lawson, *Planta Med* **55** (1989) 114–114. (https://www.thieme-connect.com/products/ejournals/abstract/10.1055/s-2006-961894)
2. S. Quintero-Fabián, D. Ortuño-Sahagún, M. Vázquez-Carrera, R. I. López-Roa, *Mediators Inflamm*. **2013** (2013). (https://doi.org/10.1155/2013/381815)
3. M. G. Jones, J. Hughes, A. Tregova, J. Milne, A. B. Tomsett, H. A. Collin, *J. Exp. Bot*. **55** (2004) 1903–1918. (https://doi.org/10.1093/jxb/erh138)
4. C. Jacob, A. Anwar, *Physiol. Plant*. **133** (2008) 469–480. (https://doi.org/10.1111/j.1399-3054.2008.01080.x)
5. N. D. Weber, D. O. Andersen, J. A. North, B. K. Murray, L. D. Lawson, B. G. Hughes, *Planta Med*. **58** (1992) 417–423. (https://www.thieme-connect.com/products/ejournals/abstract/10.1055/s-2006-961504)
6. A. Helen, K. Krishnakumar, P. L. Vijayammal, K. T. *Augusti, Pharmacology* **67** (2003) 113–117. (https://doi.org/10.1159/000067796)
7. D. A. Hanoush, A. H. Al-Auqaili, M. Mansour, A. Ghosh, Trop. *J. Nat. Prod. Res*. **6** (2022) 1233–1240. (http://www.doi.org/10.26538/tjnpr/v1i4.5)
8. J. M. Casasnovas, T. A. Springer, *J. Biol. Chem.* **270** (1995) 13216–13224. (https://doi.org/10.1074/jbc.270.22.13216)
9. P. Gale, *Microb. Risk Anal.* **21** (2022) 100198. (https://doi.org/10.1016/j.mran.2021.100198)
10. M. E. Popovic, *Microbiol. Res.* **270** (2023) 127337. (https://doi.org/10.1016/j.micres.2023.127337)
11. K. Rajagopal, G. Byran, S. Jupudi, R. Vadivelan, Int. *J. Heal. Allied Sci*. **9** (2020) 43–50. (http://www.doi.org/10.4103/ijhas.IJHAS_55_20)

12. W. Lopez-Orozco, L. H. Mendoza-Huizar, G. A. Álvarez-Romero, J. de J. M. Torres-Valencia, *Pädi Boletín Científico Ciencias Básicas e Ing. Del ICBI* **10** (2023) 126–130. (https://repository.uaeh.edu.mx/revistas/index.php/icbi)
13. M. B. M. Spera, F. A. Quintão, D. K. D. Ferraresi, W. R. Lustri, A. Magalhães, A. L. B. Formiga, P. P. Corbi, *Spectrochim. Acta - Part A Mol. Biomol. Spectrosc*. **78** (2011) 313–318. (https://doi.org/10.1016/j.saa.2010.10.012)
14. P. Geerlings, F. De Proft, W. Langenaeker, *Chem. Rev*. **103** (2003) 1793–1873. (https://doi.org/10.1021/cr990029p)
15. R. G. Pearson, *J. Chem. Educ*. **64** (1987) 561–567. (https://doi.org/10.1021/ed064p561)
16. R. G. Parr, R. A. Donnelly, M. Levy, W. E. Palke, *J. Chem. Phys*. **68** (1977) 3801–3807. (https://doi.org/10.1063/1.436185)
17. R. G. Parr, R. G. Pearson, *J. Am. Chem. Soc*. **105** (1983) 7512–7516. (https://doi.org/10.1021/ja00364a005)
18. R. G. Parr, W. Yang, *J. Am. Chem. Soc*. **106** (1984) 4049–4050. (https://doi.org/10.1021/ja00326a036)
19. R. G. Parr, *Horizons Quantum Chem*. (1980) 5–15. (https://link.springer.com/book/10.1007/978-94-009-9027-2)
20. W. Yang, W. *J. Mortier, J. Am. Chem. Soc.* **108** (1986) 5708–5711. (https://doi.org/10.1021/ja00279a008)
21. N. Godbout, D. R. Salahub, J. Andzelm, E. Wimmer, *Can. J. Chem*. **70** (2011) 560–571. (https://doi.org/10.1139/v92-079)
22. K. Raghavachari, *Theor. Chem. Accounts* **103** (2000) 361–363. (https://link.springer.com/article/10.1007/s002149900065)
23. Y. Zhao, D. G. Truhlar, *Theor. Chem. Acc*. **120** (2008) 215–241. (https://link.springer.com/article/10.1007/s00214-007-0310-x)
24. Y. Wang, X. Jin, H. S. Yu, D. G. Truhlar, X. He, *Proc. Natl. Acad. Sci. U. S. A*. **114** (2017) 8487–8492. (https://doi.org/10.1073/pnas.1705670114)
25. J. Da Chai, M. Head-Gordon, *Phys. Chem. Chem. Phys*. **10** (2008) 6615–6620. (https://doi.org/10.1039/B810189B)
26. S. Miertuš, E. Scrocco, *J. Tomasi, Chem. Phys*. **55** (1981) 117–129. (https://doi.org/10.1016/0301-0104(81)85090-2)
27. Gaussian 09, Revision A.01, Gaussian, Inc., Wallingford, CT, 2009. (https://gaussian.com/g09citation/)
28. Gaussview Rev. 3.09, Windows version. Gaussian Inc., Pittsburgh, PA. (https://gaussian.com/508_gvw/)
29. A. Allouche, *J. Comput. Chem*. **32** (2012) 174–182. (https://doi.org/10.1002/jcc.21600)
30. T. Lu, F. Chen, *J. Comput. Chem*. **33** (2012) 580–592. (https://doi.org/10.1002/jcc.22885)
31. Jorge-Finnigan, A.; Brasil, S.; Underhaug, J.; Ruíz-Sala, P.; Merinero, B.; Banerjee, R.; Desviat, L. R.; Ugarte, M.; Martinez, A.; Pérez, B. Pharmacological chaperones as a potential therapeutic option in methylmalonic aciduria cblB type. *Hum. Mol. Genet*. **18**(2013). (https://doi.org/10.1093/hmg/ddt217)
32. E. F. Pettersen, T. D. Goddard, C. C. Huang, G. S. Couch, D. M. Greenblatt, E. C. Meng, T. E. Ferrin, *J. Comput. Chem*. **25** (2004) 1605–1612. (https://doi.org/10.1002/jcc.20084)

33. BIOVIA, Dassault Systèmes, Discovery Studio Visualiser 2019, San Diego: Dassault Systèmes, 2019. (https://discover.3ds.com/discovery-studio-visualizer-download)
34. J. L. Gázquez, *J. Phys. Chem. A* **101** (1997) 4591–4593. (https://www.scielo.org.mx/scielo.php?script=sci_arttext&pid=S1870-249X2008000100002)
35. P. K. Chattaraj, (2009) 576. (https://books.google.com/books/about/Chemical_Reactivity_Theory.html?hl=es&id=n8JBNvF_2KAC)
36. F. L. Hirshfeld, *Theor. Chim. Acta* **44** (1977) 129–138. (https://link.springer.com/article/10.1007/BF00549096)
37. E. R. Johnson, S. Keinan, P. Mori-Sánchez, J. Contreras-García, A. J. Cohen, W. Yang, *J. Am. Chem. Soc*. **132** (2010) 6498–6506. (https://doi.org/10.1021/ja100936w)
38. M. Chebaibi, D. Bousta, R. F. B. Goncalves, H. Hoummani, S. Achour, *Res. Sq*.**1** (2021). (https:// https://doi.org/10.21203/rs.3.rs-679827/v1)
39. Z. Jin, X. Du, Y. Xu, Y. Deng, M. Liu, Y. Zhao, *Nature* **582**(2020) 289-293. (https://doi.org/10.1038/s41586-020-2223-y)
40. A. Castro-Alvarez, A. M. Costa, J. Vilarrasa, *Molecules* **22** (2017). (https://doi.org/10.3390/molecules22010136).